

SCIENTIFIC REPORTS



OPEN

Therapeutic efficacy of apelin on transplanted mesenchymal stem cells in hindlimb ischemic mice *via* regulation of autophagy

Received: 23 September 2015

Accepted: 02 February 2016

Published: 23 February 2016

Dong Liang^{1,3,*}, Dong Han^{1,2,*}, Weiwei Fan^{1,4}, Ran Zhang¹, Hongyu Qiao², Miaomiao Fan², Tao Su², Sai Ma², Xiujuan Li², Jiangwei Chen², Yabin Wang¹, Jun Ren⁵ & Feng Cao^{1,2}

Mesenchymal stem cells (MSCs)-based therapy provides a promising avenue for the management of peripheral arterial disease (PAD). However, engrafted MSCs are subjected to acute cell death in the ischemic microenvironment. Apelin has been shown to protect bone marrow MSCs against apoptosis although the mechanism of action remains elusive. Here we demonstrated that apelin promoted functional survival of AD-MSCs in ischemic hindlimbs and provoked a synergetic effect with AD-MSCs to restore hindlimb blood perfusion and limb functions. Further *in vitro* studies revealed that a biphasic response in autophagy was induced by apelin in AD-MSCs during hypoxia and hypoxia/reoxygenation (H/R) stages to exert cytoprotective effects against H/R injury. Mechanistically, apelin increased the viability of AD-MSCs via promoting protective autophagy during hypoxia, which was accompanied with activation of AMPK and inhibition of mammalian target of rapamycin (mTOR). To the contrary, apelin suppressed autophagic cell death during reoxygenation, which was accompanied with activation of Akt and inhibition of Beclin1. Our findings indicated that apelin facilitated AD-MSCs-based therapy in PAD, possibly through promoting survival of AD-MSCs by way of autophagy regulation. Our data support the promises of apelin as a novel strategy to improve MSC-based therapy for PAD, possibly through autophagy modulation in MSCs.

Peripheral arterial disease (PAD) remains one of the leading causes of deformity worldwide¹. Among various therapeutic options for PAD, stem cell-based therapies hold some great promises in the management of PAD². Nonetheless, the therapeutic efficacy has been held back by the poor survival of donor cells³. Our previous findings also demonstrated the feasibility of utilizing adipose derived mesenchymal stem cells (AD-MSCs) in the management of PAD courtesy of its multipotency, abundance for harvest and low immunogenicity⁴. However, low survival rate has been identified for the transplanted AD-MSCs within ischemic tissues, hampering the advancement of AD-MSCs in the therapeutics of PAD⁴. To this end, it is pertinent to search for new and novel approaches to promote donor cell survival in order to foster the success of stem cell-based therapy for PAD.

Stem cells drastically differ from somatic cells in their ability of self-renewal and multi-directional differentiation. Due to their relatively long life in the organisms, it is conceived that the cell sweeper autophagy should be indispensable for quality control and maintenance of cellular homeostasis for stem cells^{5,6}. In spite of the rich knowledge available for somatic cells, the precise role for autophagy in the maintenance and function of stem cells is only beginning to be understood as a result of some recent seminal studies^{7,8}. Moreover, previous work has been mainly focused on modulation of inflammation and oxidative stress in ischemic microenvironment to improve the survival of engrafted MSCs^{9,10}. Autophagy, an important regulator of cellular function and survival, was rarely examined and its role was often omitted for the survival of engrafted MSCs in ischemic condition. Accumulating

¹Department of Cardiology, Chinese PLA General Hospital, Beijing, 100853, China. ²Department of Cardiology, Xijing Hospital, Fourth Military Medical University, Xi'an, Shaanxi 710032, China. ³Department of Cardiology, Armed Police Corps Hospital of Shaanxi, Xi'an, Shaanxi 710032, China. ⁴Department of Cardiology, the 175th Hospital of Chinese PLA, the Affiliated Southeast Hospital of Xiamen University, Zhangzhou, Fujian 363000, China. ⁵Center for Cardiovascular Research and Alternative Medicine, University of Wyoming, Laramie, WY 82071, USA. *These authors contributed equally to this work. Correspondence and requests for materials should be addressed to J.R. (email: jren@uwyo.edu) or F.C. (email: wind8828@gmail.com)

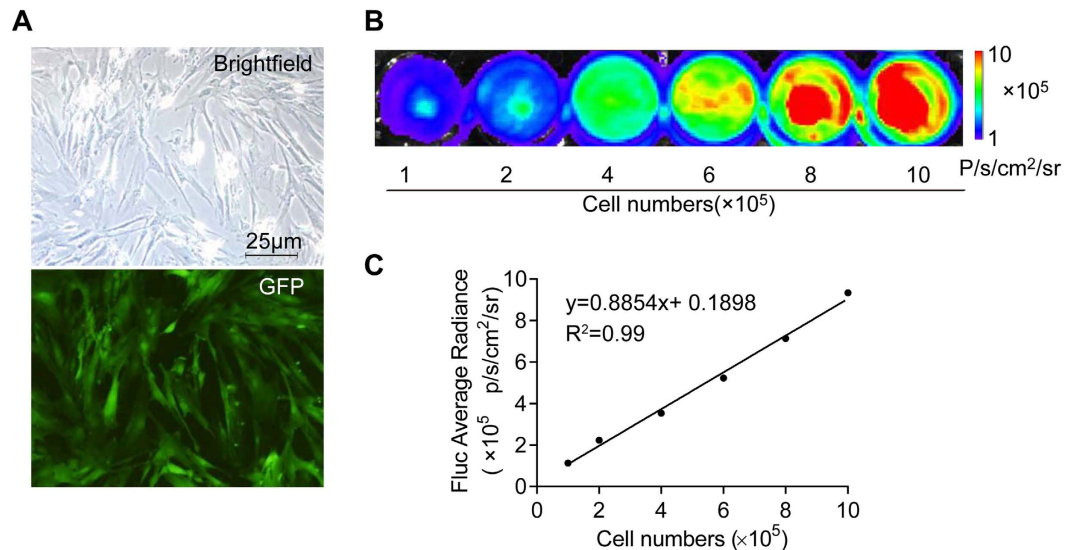


Figure 1. Morphology and BLI images of AD-MSCs *in vitro*. (A) Morphology of the third-passage AD-MSCs cultured *in vitro* (up); AD-MSCs is GFP positive (lower panel). (B) BLI with different numbers of AD-MSCs. (C) A linear relationship is depicted between AD-MSCs numbers and BLI signal intensity; Scale bar: 25 μm.

evidence has consolidated for a major role of autophagy, a cellular process involved in protein and organelle degradation, in a variety of physiological processes, including inflammation, oxidative stress, autophagic cell death and immune responses^{11,12}. Recent evidence also suggested that autophagy may serve as a therapeutic target in the management of ischemia/reperfusion injury¹³. While low levels of autophagy exhibit a cyto-protective role, high levels or sustained autophagy may promote cell injury and irreversible cell death (type 2 programmed cell death)¹⁴. Not surprisingly, targeting the pro-death and pro-survival routes in the regulation of autophagy has drawn much attention for the management against ischemic diseases.

Apelin (also known as APLN) is a peptide encoded by the *apelin* gene. The *apelin* gene encodes a 77 amino acid preproprotein which can be further cleaved to shorter biologically active fragments, including apelin-12, apelin-13, apelin-16, apelin-17, and apelin-19. Ample of evidence has indicated that the pyroglutamated form of apelin-13 (Pyr-apelin-13) may be the most potent isoform of apelin to serve as the principal biologically active ligand^{15,16}. The apelin receptor (also known as the APJ receptor) is a G protein-coupled receptor which binds apelin molecule. Apelin is ubiquitously expressed in various organs such as the heart, lung, kidney, liver, adipose tissue, gastrointestinal tract, brain, adrenal glands, endothelium and plasma^{17,18}. Apelin has been demonstrated to exhibit cyto-protective effects against both cardiac and cerebral ischemic injuries^{19–21}. In particular, apelin was found to protect against serum deprivation-induced apoptosis in cultured rat bone marrow mesenchymal stem cells²². Given that apelin is known to participate in the regulation of autophagy^{23,24}, the present study was designed to examine the impact of apelin on the survival of transplanted AD-MSCs in a murine hindlimb ischemia model and the underlying mechanisms involved with a focus on autophagy.

Results

Morphology and bioluminescence imaging (BLI) of AD-MSCs^{Fluc+GFP+}. AD-MSCs^{Fluc+GFP+} cultured in medium displayed a fibroblast-like morphology (Fig. 1A-a). AD-MSCs^{Fluc+GFP+} were positive for eGFP (enhanced green fluorescent protein) under fluorescent microscope (Fig. 1A-b). The stable expression of firefly luciferase (Fluc) was confirmed by bioluminescence imaging (BLI) in AD-MSCs (Fig. 1B). Moreover, cells expressed Fluc reporter gene in a number-dependent fashion as confirmed by BLI. The BLI signal intensity of 1.0×10^5 to 1.0×10^6 AD-MSCs rose gradually from 1.12×10^5 to 9.33×10^5 p/s/cm²/Sr. A linear correlation was identified between cell quantities and Fluc signal (correlation coefficient: 0.99; linear regression equation: $y = 0.8854x + 0.1898$) (Fig. 1C). These data indicated that BLI of Fluc may serve as a reliable tool to monitor viable transplanted AD-MSCs quantitatively *in vivo*.

Restoration of hindlimb blood perfusion in PAD model following AD-MSCs transplantation and apelin administration. *In vivo* laser Doppler perfusion imaging (LDPI) visualized the dynamic changes in hindlimb blood perfusion (Fig. 2A). Perfusion ratio (PR), i.e., the ratio of average LDPI, an index of ischemic to nonischemic hindlimbs, was quantified to evaluate the hindlimb blood perfusion status. As shown in Fig. 2A,B, there was little difference in PR between groups on postoperative day (POD) 0 ($p > 0.05$). PR rose gradually in both groups over the next few days. Mice exhibited a higher perfusion ratio in ischemic hindlimbs in both AD-MSCs and apelin groups compared with that of PBS group (Fig. 2B), with a much more pronounced improvement from combined therapy of AD-MSCs and apelin. PR was significantly higher in AD-MSCs + apelin group than AD-MSCs or apelin group (Fig. 2B).

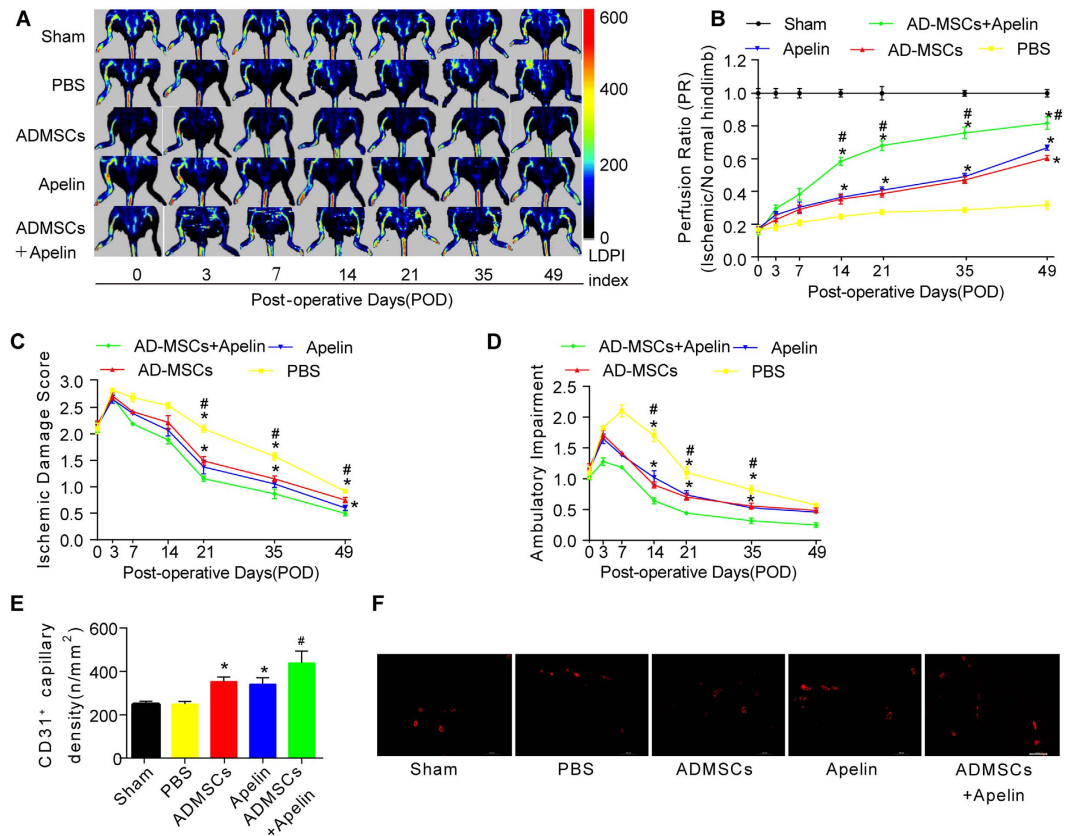


Figure 2. AD-MSCs transplantation and apelin administration promoted hindlimb functional recovery and angiogenesis in the PAD model. (A,B) *In vivo* laser Doppler perfusion imaging (LDPI) visualized dynamic changes in hindlimb blood perfusion, which was (B) quantified using perfusion ratio (PR), i.e., the ratio of average LDPI index of ischemic (left leg, red arrows, the same to fig. 4A) to nonischemic hindlimbs. Colored scale bar represents blood flow velocity in LDPI index. $n = 10$. (C,D) Cumulative results for functional assessment of ischemic muscle over follow-up are shown graphically as ischemic damage score (C) and ambulatory impairment score (D), $n = 15$ for each group. (E,F) Representative image and quantitative analysis of the CD31-positive blood vessels within the same-sized regions of adductor muscle section among groups, as assessed by immunofluorescence staining with endothelial marker CD31 (PECAM-1) on POD49. $n = 20$ random fields. Error bars represent mean \pm SD. * $P < 0.05$ vs. PBS, # $P < 0.05$ vs. both AD-MSCs and apelin. Scale bar: 100 μ m.

Hindlimb functional recovery in PAD model following AD-MSCs transplantation and apelin administration. To reveal hindlimb functional recovery, blind scoring of semi-quantitative assessment of impaired use of murine ischemic limb was performed as described in the method section. As shown in Fig. 2C,D, there was no significant difference in ischemic damage and ambulatory impairment scores between experimental groups on POD 0. Ischemic damage and ambulatory impairment scores gradually dropped over the next few days beyond POD7. Blind scoring depicted that both AD-MSCs and apelin ameliorated ischemic damage and ambulatory impairment compared with that of PBS group (Fig. 2C,D), while combined therapy of AD-MSCs and apelin further improved functional recovery of ischemic hindlimbs (Fig. 2C,D).

Hindlimb angiogenesis in PAD model following AD-MSCs transplantation and apelin administration. On POD 49, 5 mice from each group were sacrificed for histological staining for CD31. Histological staining analysis indicated that both AD-MSCs and apelin improved the density of CD31-positive vessels compared with that of PBS group (Fig. 2E), while combined therapy of AD-MSCs and apelin further improved the density of the CD31-positive vessels in ischemic hindlimbs (Fig. 2E).

Survival of engrafted AD-MSCs^{Fluc+GFP+} in murine model of PAD. Noninvasive BLI longitudinally revealed the fate of AD-MSCs transplanted into ischemic hindlimbs (Fig. 3A). After initial cell transplantation for 7 days, the BLI signal intensity reached peak. BLI signal exhibited little significant difference among different groups prior to POD3 ($P > 0.05$). However, BLI signal intensity of engrafted AD-MSCs in the Sham + AD-MSCs and AD-MSCs groups experienced a progressive decline in the following 6 weeks, with a decrease in BLI signal from $(12.3 \pm 0.14) \times 10^5$ p/s/cm²/sr and $(12.1 \pm 0.18) \times 10^5$ p/s/cm²/sr respectively on POD0 to $(7.4 \pm 0.57) \times 10^5$ p/s/cm²/sr and $(10.72 \pm 2.28) \times 10^5$ p/s/cm²/sr respectively on POD14, to the background levels on POD49 (Fig. 2B). Apelin treatment improved AD-MSCs survival *in vivo*. In Sham + AD-MSCs + apelin

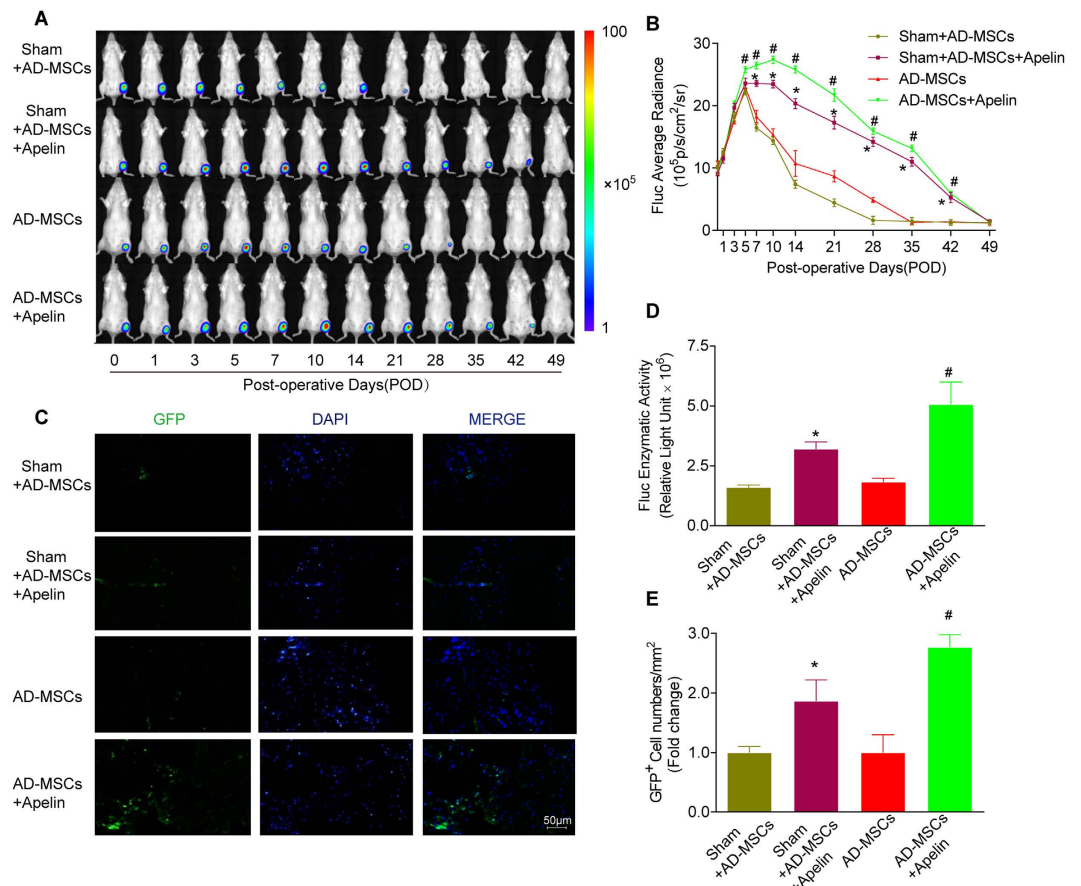


Figure 3. Survival of the grafted AD-MSCs^{Fluc+GFP+} in murine ischemic hindlimbs following apelin treatment. (A,B) Longitudinal BLI spatiotemporally tracked AD-MSCs^{Fluc+GFP+} survival *in vivo* (n = 10 for each group). Quantitative analysis of (B) *in vivo* Fluc optical signals demonstrated the progressive death of AD-MSCs^{Fluc+GFP+} following transplantation. Colored scale bar represents BLI radiance intensity in P/s/cm²/sr. (C) Confocal microscopy of adductor muscle tissue sections with double immunofluorescence staining of GFP (green), and 4',6-diamidino-2-phenylindole (DAPI, blue) for nuclei as indicated on POD14. (D) *Ex vivo* Fluc enzymatic activity on POD14 (n = 5). (E) More GFP-positive cells were observed in the apelin treated group than non-apelin treated group (n = 20 random fields). Error bars represent mean ± SD. Scale bars represent 50 μm. *P < 0.05 vs. Sham + AD-MSCs, #P < 0.05 vs. AD-MSCs.

and AD-MSCs + apelin group, donor AD-MSCs exhibited significantly enhanced survival, as evidenced by a remarkably higher BLI signal intensity than their respective non-apelin-treated groups on POD35 (Fig. 3B). This was also confirmed by the significantly higher Fluc enzymatic activity in the apelin-treated groups compared with their respective non-apelin-treated groups on POD14 (Fig. 3D). Moreover, laser confocal microscopy displayed more GFP-positive AD-MSCs within the ischemic tissues in apelin-treated groups on POD14 compared with their respective non-apelin-treated group (Fig. 3C,E).

The PI3K inhibitor LY294002 abolished the beneficial effects of apelin on ischemic hindlimb recovery and AD-MSCs survival. We further examined the possible involvement of AMPK and Akt signaling pathways in the pro-survival effect of apelin on AD-MSCs in ischemic hindlimbs. LDPI revealed that the PI3K inhibitor LY294002 but not the AMPK inhibitor compound C abolished the beneficial effects of apelin and AD-MSCs on restoration of hindlimb blood perfusion (Fig. 4A,B). Likewise, LY294002 also abolished the beneficial effects of apelin and AD-MSCs on hindlimb functional recovery as evidenced by the semi-quantitative assessment for ischemic damage and ambulatory impairment scores (Fig. 4C,D). Hindlimb angiogenesis property of AD-MSCs and apelin was reversed by LY294002 as evidenced by histological staining analysis of the CD31-positive vessel density (Fig. 4E). In contrast, these responses were unaffected by the AMPK inhibitor compound C.

Our data further revealed that survival of engrafted AD-MSCs was inhibited by LY294002. BLI assay demonstrated that the PI3K inhibitor LY294002 but not the AMPK inhibitor compound C reversed the pro-survival effect of apelin on AD-MSCs *in vivo*. In AD-MSCs + apelin + LY294002 group, donor AD-MSCs exhibited an early trend of cell death, manifested by remarkably lower BLI signal intensity compared with that from the AD-MSCs + apelin group (Fig. 4F,G).

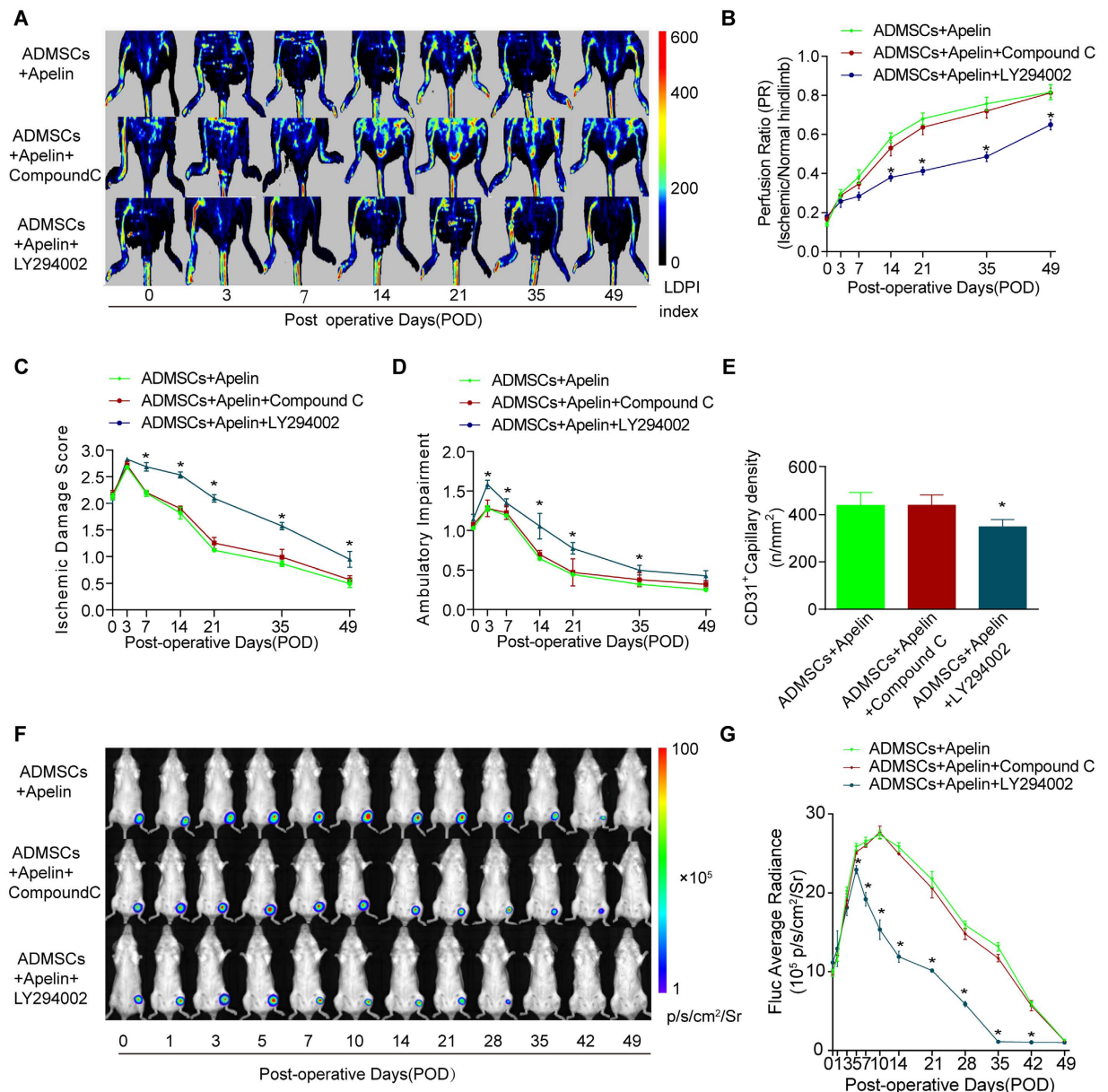


Figure 4. The PI3K inhibitor LY294002 abolished the beneficial effects of apelin on ischemic hindlimb recovery and AD-MSCs survival. (A,B) *In vivo* laser doppler perfusion imaging (LDPI) visualized the dynamic changes in hindlimbs blood perfusion, which was (B) quantified using perfusion ratio (PR). $n = 10$. (C,D) Cumulative results for functional assessment of ischemic muscle over follow-up are shown graphically as ischemic damage score (C) and ambulatory impairment score (D), $n = 15$ for each group. (E) Quantitative analysis of the CD31-positive blood vessels within the same-sized regions of adductor muscle section among groups, as assessed by immunofluorescence staining with endothelial marker CD31 (PECAM-1) on POD49. $n = 20$ random fields. (F,G) Longitudinal BLI spatiotemporally tracked AD-MSCs^{Fluc+GFP+} survival *in vivo* ($n = 9$ for each group). Quantitative analysis of (G) *in vivo* Fluc optical signals demonstrated that LY294002 but not compound C abolished the beneficial effects of apelin on AD-MSCs survival. * $P < 0.05$ vs. AD-MSCs + apelin.

Apelin regulated autophagy in AD-MSCs under hypoxia and hypoxia/reoxygenation injury *in vitro*.

To further discern the mechanisms of autophagy behind the pro-survival effects of apelin on AD-MSCs, an *in vitro* hypoxia/reoxygenation (H/R) model was employed to simulate the ischemic hindlimb model *in vivo*. Autophagy level of AD-MSCs was assessed using protein expression of microtubule-associated protein 1 light chain3 (LC3) and SQSTM1 (p62) under hypoxia and H/R at different time points. Both hypoxia and hypoxia/reoxygenation treatments increased the ratio of LC3II/I compared with the normoxia group in all experimental conditions, along with a gradual decrease in p62 protein levels (Fig. 5A,B). Furthermore, apelin (10^{-6} M) treatment promoted autophagy in AD-MSCs under hypoxia (increased ratio of LC3II/I and decreased p62 protein levels compared with the non-apelin treated group (Fig. 5C,D), while the elevated autophagy in

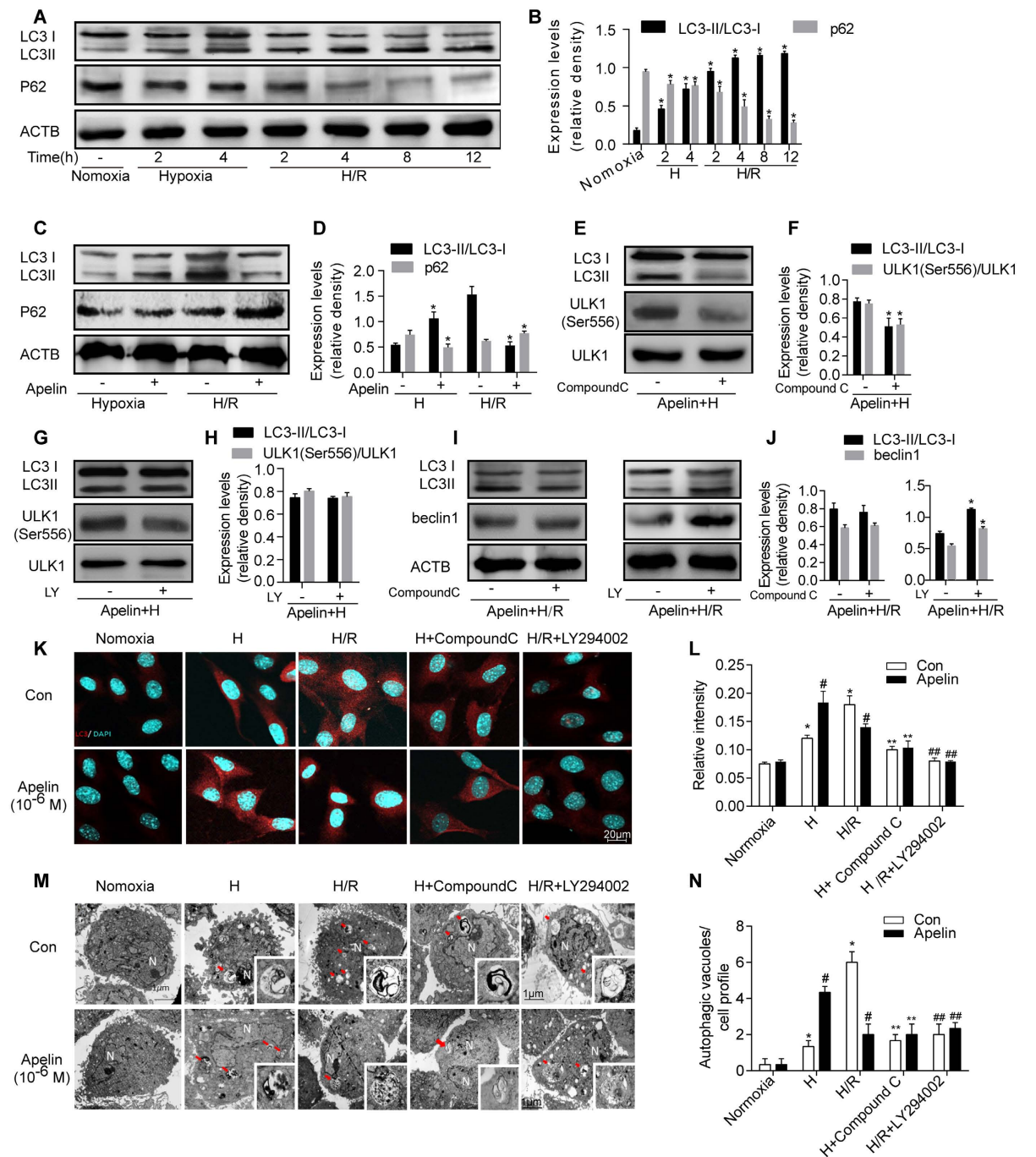


Figure 5. Apelin regulated autophagy in AD-MSCs under hypoxia and hypoxia/reoxygenation injury *in vitro*. (A) Representative gel bolts depicting LC3 and p62 protein expression under hypoxia and hypoxia/reoxygenation injury *in vitro* at different time points. (B) Quantitative analysis of A. * $p < 0.05$ compared with normoxia group. (C) Representative gel bolts depicting LC3 and p62 protein expression regulated by apelin under hypoxia and hypoxia/reoxygenation injury. (D) Quantitative analysis of C. * $p < 0.05$ compared with respective non-apelin treated group. (E–J) Representative gel bolts and respective quantitative analysis of LC3, p-ULK1, and Beclin1 expression. Cells were pretreated with apelin (10^{-6} M) in the presence or absence of AMPK inhibitor compound C ($10 \mu\text{M}$) or PI3K inhibitor LY294002 ($20 \mu\text{M}$) for 4 h, followed by hypoxia (4 h) or hypoxia (4 h) /reoxygenation (12 h). * $p < 0.05$ compared with respective non-compound C or non-LY294002 treated group. (K,L) Representative immunofluorescence staining of LC3 under confocal microscopy. (L) Quantitative analysis of K ($n = 10$ random fields). * $p < 0.05$ compared with normoxia group, # $p < 0.05$ compared with respective non-apelin treated group, ** $p < 0.05$ compared with respective hypoxia group, ## $p < 0.05$ compared with respective H/R group. (M, N) Representative Transmission electron microscopy(TEM) images of AD-MSCs after treatment as described in (E). (N) Quantitative analysis of M ($n = 10$ random fields), * $p < 0.05$ compared with respective non-apelin treated group, ** $p < 0.05$ compared with respective hypoxia group, ## $p < 0.05$ compared with respective H/R group. LY represents LY294002.

AD-MSCs under H/R was abrogated by apelin (10^{-6} M) treatment (manifested as the decreased ratio of LC3II/I and increased p62 protein level compared with non-apelin-treated group) (Fig. 5C,D).

Next, to further explore the regulatory mechanisms of autophagy behind apelin, the AMPK inhibitor compound C ($10\ \mu\text{M}$) or the PI3K inhibitor LY294002 ($20\ \mu\text{M}$) was administered to AD-MSCs. Result showed that under hypoxia, the apelin-enhanced autophagy and phosphorylation of ULK1 were reversed by compound C but not LY294002 (Fig. 5E–H). To the contrary, the apelin-suppressed autophagy and Beclin1 expression under H/R were reversed by LY294002 but not compound C (Fig. 5I,J).

To further consolidate apelin-induced autophagy in AD-MSCs, immunofluorescent staining and transmission electron microscope were performed for LC3 and phagophore-autophagosome visualization, respectively. Immunofluorescence of LC3 depicted that LC3 expression was elevated by both hypoxia and H/R compared with normoxia group (Fig. 5K,L). Interestingly, apelin promoted and suppressed autophagy in hypoxia and H/R, respectively (Fig. 5K,L). While compound C abrogated apelin-induced increase in LC3 expression under hypoxia, LY294002 abrogated apelin-suppressed LC3 expression under H/R (Fig. 5K,L). Moreover, transmission electron microscopy (TEM), the most reliable technique for qualitative assessment of autophagy, exhibited similar pattern of autophagy regulation under hypoxia and H/R conditions. Hypoxia and H/R increased number of vacuoles compared with normoxia group (Fig. 5M,N). Consistent with the immunofluorescent staining result, apelin promoted and suppressed autophagy under hypoxia and H/R, respectively (Fig. 5M,N). Likewise, compound C abrogated apelin-induced increase in the number of vacuoles under hypoxia while LY294002 nullified apelin-elicited loss in the number of vacuoles under H/R (Fig. 5M,N).

Differential autophagy effect in AD-MSCs survival under hypoxia or hypoxia/reoxygenation. 3-(4,5-dimethylthiazol-2-yl)-2,5-diphenyltetrazolium bromide (MTT) assay and *in vitro* BLI were conducted to evaluate cell viability. Hypoxia and H/R significantly decreased cell viability, the effect of which was attenuated by apelin (10^{-8} and 10^{-6} M). In fact, apelin pretreatment significantly increased cell viability in normoxia, hypoxia and H/R conditions (Fig. 6A).

To discern a role for autophagy in apelin-induced AD-MSCs survival, AD-MSCs cells were pretreated with or without apelin (10^{-6} M) for 24 h. AD-MSCs were then subjected to 4-hour hypoxia followed by 12-hour reoxygenation (H/R) in the presence or absence of the autophagy inhibitor 3-MA ($10\ \text{mM}$) or the autophagy inducer rapamycin (Rapa, $5\ \mu\text{M}$). Our data revealed that hypoxia significantly decreased the cell viability, the effect of which was attenuated by apelin. 3-MA significantly enhanced hypoxia-induced AD-MSCs death while mitigating the protective role of apelin. On the other hand, rapamycin effectively rescued hypoxia-induced cell death in a manner reminiscent of apelin. Furthermore, H/R greatly lessened cell survival although with a much less pronounced effect in the apelin-treated group. Interestingly, 3-MA significantly attenuated H/R-elicited cell death in a manner similar to apelin, whereas rapamycin greatly aggravated H/R-induced cell death in both control and apelin groups. These data suggest a likelihood paradoxical role for autophagy in apelin-induced cytoprotection under hypoxia and H/R (Fig. 6B–F).

AMPK and Akt signaling pathways involved in autophagy during hypoxia and hypoxia/reoxygenation *in vitro*. Mammalian target of rapamycin (mTOR) serves as a critical signaling regulator for autophagy under the positive and negative control of Akt and AMPK, respectively. Protein expression of AMPK, Akt, and mTOR *etc.* was assessed along with autophagy under hypoxia and reoxygenation at different time points. Our data revealed a significant concurrent increase in ULK1 and AMPK phosphorylation under hypoxia in AD-MSCs, which was accompanied by a decline in the phosphorylation of mTOR (Fig. 7A,B). These responses in the phosphorylation of ULK1, AMPK and mTOR were augmented by apelin (10^{-6}M) treatment (Fig. 7A,D). Our further findings revealed a significant decrease in Akt phosphorylation and Bcl2 during reoxygenation, which was accompanied by an increase in Beclin1 (Fig. 7A,C). These responses were reversed by apelin (10^{-6}M) treatment (Fig. 7A,E). These findings suggested a likely disparate role of autophagy in the apelin-offered cytoprotection against hypoxia and H/R involving AMPK-mTOR-ULK1 signaling in hypoxia phase along with Akt-Bcl2-Beclin1 signaling in reoxygenation phase (Fig. 8).

Apelin induced eNOS phosphorylation during hypoxia and hypoxia/reoxygenation *in vitro*. To achieve a better understanding of the apelin-elicited cytoprotective effects, we evaluated eNOS phosphorylation in MSCs. Our results shown in supplementary figure revealed that apelin enhanced eNOS phosphorylation in AD-MSCs in hypoxia injury as well as in hypoxia/reoxygenation period ($p < 0.05$), suggesting a possible role of eNOS in apelin-elicited cytoprotection.

Discussion

Recently, MSCs have been reported to undergo autophagy which is expected to dictate the therapeutic potential of MSCs in experimental autoimmune encephalomyelitis²⁵. Here we demonstrated that apelin-elicited MSCs autophagy contributed to elevated functional survival of AD-MSCs in ischemic hindlimbs and eventually led to enhanced AD-MSCs therapeutic potential in experimental PAD. Ischemic context severely impairs the survival and retention of AD-MSCs in targeted sites. Modulation of autophagy by apelin drastically improved the functional survival and therapeutic efficacy of AD-MSCs in experimental PAD. This effect of apelin was associated with enhanced protective autophagy in hypoxia phase and decreased autophagic cell death in H/R phase. We further revealed that AD-MSCs autophagy during hypoxia phase is mediated through AMPK/mTOR/ULK1 pathway, which was up-regulated by apelin. On the other side of the coin, H/R energized autophagic cell death through an Akt/Bcl2/Beclin1-dependent pathway, which was likely down-regulated by apelin. This biphasic regulation of AD-MSCs autophagy by apelin might account for the enhanced therapeutic potential of apelin in AD-MSCs-based experimental PAD. Our findings suggest that modulation of autophagy in MSCs by apelin may

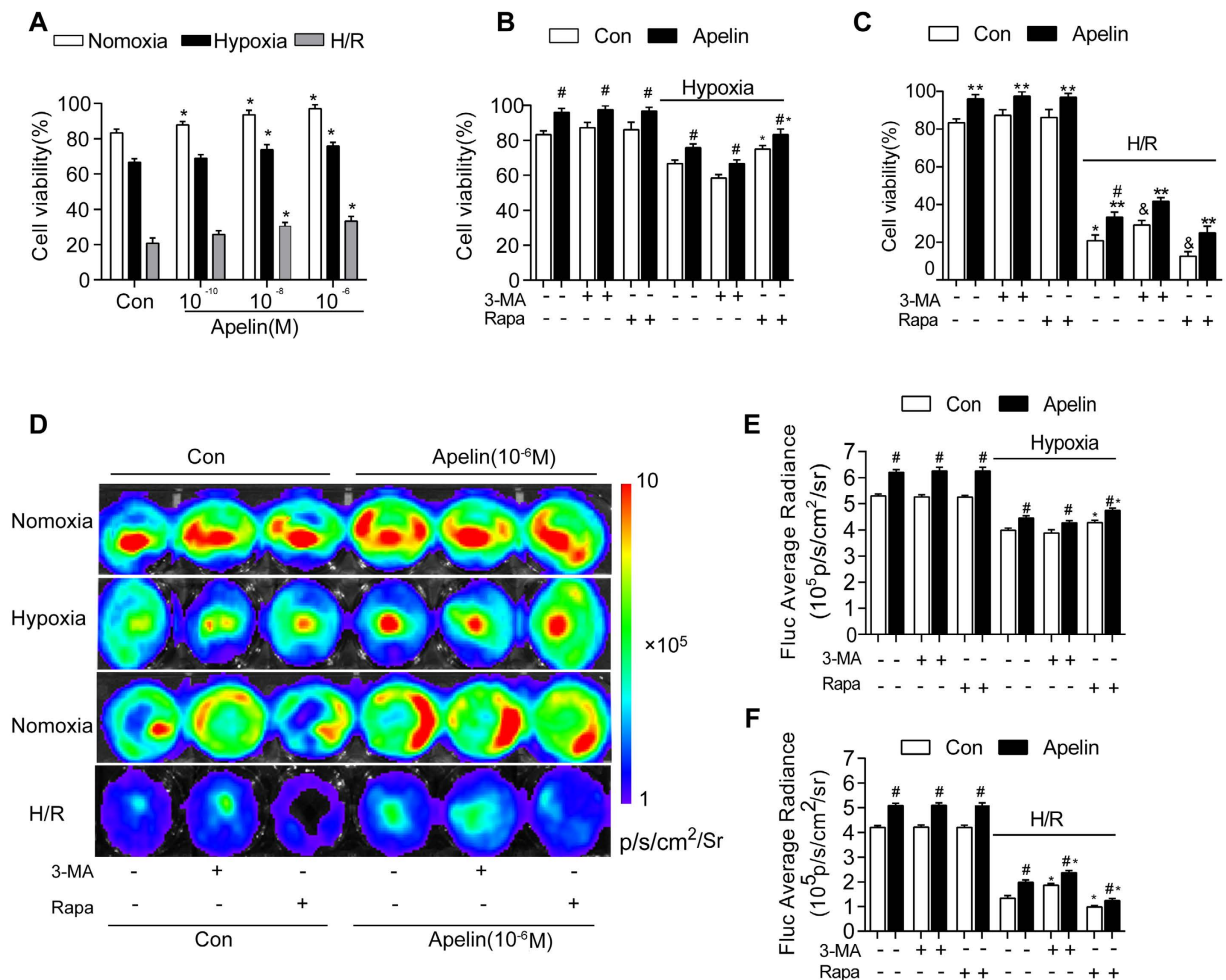


Figure 6. Differential autophagy effect in AD-MSCs survival under hypoxia or hypoxia/reoxygenation.

(A) Cell viability of AD-MSCs following hypoxia–reoxygenation and different dose of Apelin pretreatment was examined using MTT assay. * $p < 0.05$ compared with respective control group. (B,C) AD-MSCs were pretreated with or without apelin (10^{-6} M) for 24 h. AD-MSCs were then subjected to a 4 hours hypoxia followed with or without a 12 hours reoxygenation (H/R) in the presence or absence of the autophagy inhibitor 3-MA (10 mM) or the autophagy inducer rapamycin (Rapa, 5 μ M). Cell viability of AD-MSCs following treatment was examined using MTT assay. * $p < 0.05$ compared with respective control group without apelin treatment. * $p < 0.05$ compared with respective control group without inhibitor treatment. (D) Representative BLI images of AD-MSCs after treatment as described in (B). (E–F) Quantitative analysis of Fluc signal in (D) ($n = 5$). * $p < 0.05$ compared with respective control group without apelin treatment. * $p < 0.05$ compared with respective control group without inhibitor treatment.

present a novel strategy to improve MSCs therapeutic efficacy in experimental PAD and other ischemic disorders in a much broader context.

Ample preclinical and clinical studies have demonstrated that cell survival and retention is closely related to the outcome of MSC-mediated therapy^{25,26}. For example, Vrtovec and colleagues revealed that improvement of left ventricular ejection fraction (LVEF) was closely correlated with the cell retention in CD34⁺ peripheral blood mononuclear cells (PBMNCs) mediated therapy for dilated cardiomyopathy (DCM)²⁵. Silva and coworkers demonstrated that functional recovery for the heart was partially determined by cell retention in bone marrow mononuclear cells (BMMNCs) mediated therapy for ST elevation myocardial infarction (STEMI)²⁶. Moreover, the surviving fraction of donor cells is quite variable in different studies, ranging from 0% to 90%, contributing to the continuing uncertainty for the therapeutic efficacy^{27,28}. To this end, improving cell survival and retention is pertinent to promote the therapeutic efficacy of MSCs in PAD therapy. Taking advantage of BLI, we longitudinally and spatiotemporally visualized the abbreviated lives of AD-MSCs following their transplantation into murine ischemic hindlimbs *in vivo*, or following H/R insult *in vitro*, which should provide favorable benefits in non-invasive cell tracking of AD-MSCs *in vivo*. Our BLI observation has consolidated that apelin may enhance the functional survival of AD-MSCs in experimental PAD, thus providing a promising measure for future stem cell-based therapy in ischemic diseases.

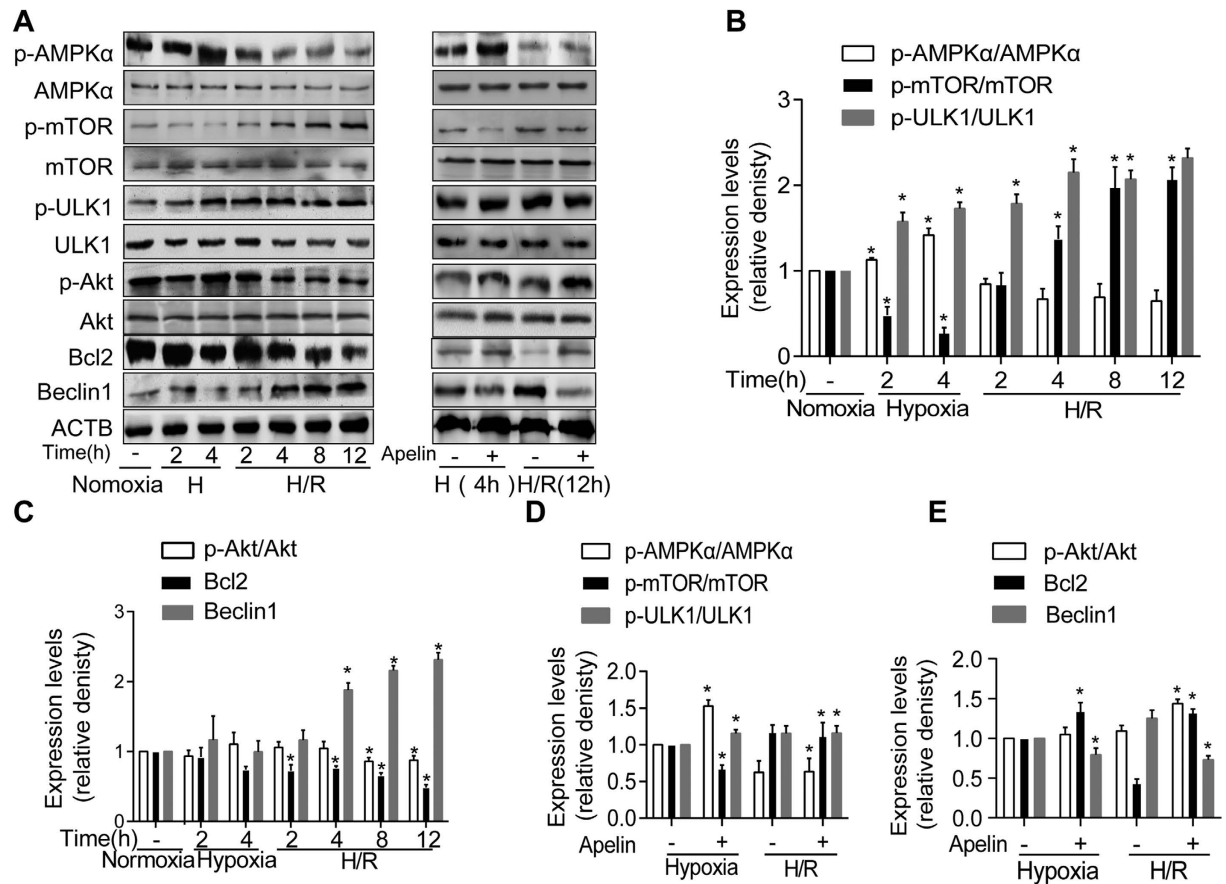


Figure 7. AMPK and Akt signaling pathways in AD-MSCs during hypoxia and hypoxia/reoxygenation *in vitro*. (A) Representative gel bolts depicting protein expressions under hypoxia and hypoxia/reoxygenation injury and apelin treatment. (B,C) Quantitative analysis of the Western blots. * $p < 0.05$ compared with normoxia group. (D,E) Quantitative analysis of the Western blots. * $p < 0.05$ compared with respective non-apelin treated group.

Previous evidence has indicated the feasibility of apelin in the treatment of PAD. Apelin is reported to be up-regulated following myocardial ischemia to turn on the reperfusion injury salvage kinase pathway, en route to a delay in the mitochondrial permeability transition pore opening and protection against ischemic cardiac injury²⁹. On the other hand, apelin was suggested to enhance cardiac neovascularization after myocardial infarction³⁰. This seems to fit well with the promising role for therapeutic angiogenesis in the management of PAD. Recent growing evidence has depicted the safety and efficacy of therapeutic angiogenesis using gene and cell therapy³¹. Our previous work demonstrated that AD-MSCs transplantation exhibited great potential in the management of PAD³². In our present work, apelin is proved to possess a synergetic effect with AD-MSCs to improve AD-MSCs-mediated limb repair following ischemic hindlimb injury.

A tie has been suggested for apelin and stem cell proliferation. Li and colleagues reported that the apelin/APJ signaling pathway might be involved in hypoxia-induced BMSC (bone marrow stem cells) proliferation³³. Their findings revealed a possible role for apelin in the processes of BMSC proliferation through the Akt/GSK3 β CyclinD1 pathway³⁴. Similarly, apelin has been reported to promote hypoxia-induced proliferation of endothelial progenitor cells and to increase myocardial progenitor cells following myocardial infarction^{35,36}. In fact, apelin possessed mitogenic effects on a wide variety of cell types and was capable of stimulating the growth or proliferation of many different cell types including human umbilical vein endothelial cells³⁷, human vascular smooth muscle cells³⁸. Consistent with these reports, our current findings revealed a rather crucial role for apelin in the proliferation and survival of AD-MSCs subjected to hypoxia and hypoxia/reoxygenation injury, possibly through autophagy regulation in AD-MSCs.

A large amount of evidence supported that autophagy was closely related to cell survival or cell death³⁹. On one hand, agents capable of inducing autophagy have been found to be cytoprotective, such as rapamycin and statins^{7,40}. On the other hand, autophagy may also promote cell death⁴¹. It is generally conceived that moderate autophagy may be cytoprotective while excessive autophagy may result in autophagic cell death¹⁴. Our data showed that apelin treatment facilitates autophagy in hypoxia phase and inhibits autophagy in reoxygenation phase. Likewise, inhibition of autophagy abrogated cytoprotective properties of apelin in AD-MSCs during hypoxia, while inhibition of autophagy promoted the pro-survival capacity of apelin during reoxygenation. Therefore, although hypoxia-induced autophagy in AD-MSCs may be protective in general, it turned out to be

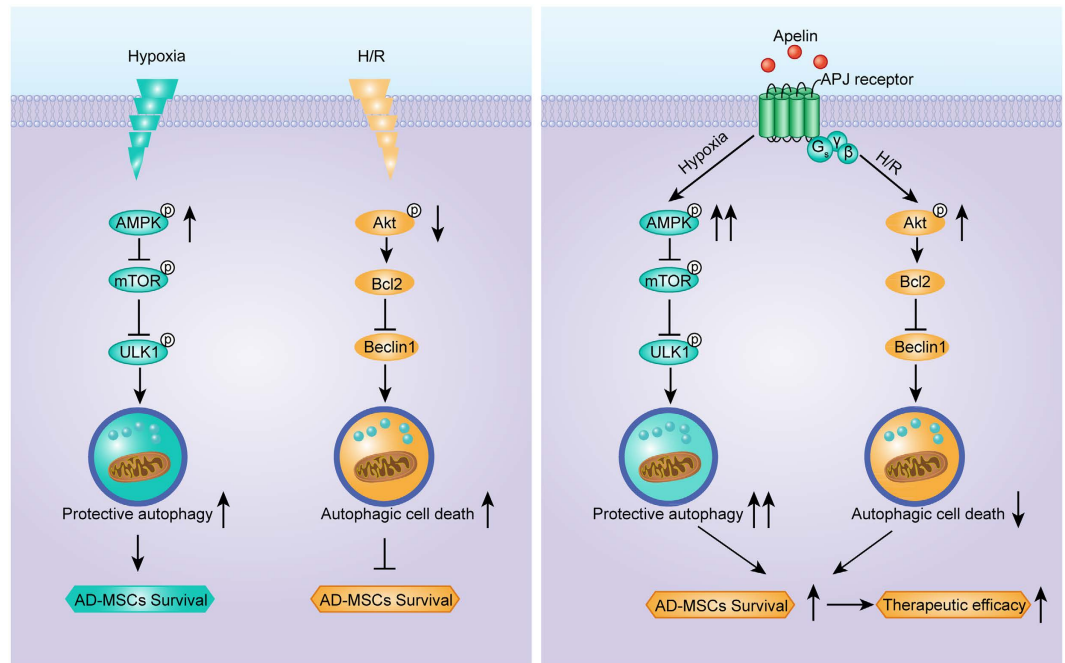


Figure 8. Schematic diagrams depicting apelin regulation of AD-MSCs autophagy under hypoxia and H/R.

Hypoxia stimulates AMPK activation and mTOR inhibition in MSCs, leading to a mild elevation of protective autophagy, and promoted MSCs survival in an autophagic aspect (the direct and overall effect of hypoxia is detrimental for MSCs survival), while apelin enhanced AMPK activation, mTOR inhibition, subsequent protective autophagy and AD-MSCs survival in hypoxia phase. On the other hand, H/R leads to a decreased activation of Akt and Bcl2 in MSCs, increasing the level of autophagic cell death, and impairs MSCs survival, while apelin enhanced activation of Akt and Bcl2 in MSCs, leading to suppression of autophagic cell death in H/R. Apelin exhibited the potential to enhance survival of engrafted MSCs via regulation of MSCs autophagy. Thus, apelin may be a potential target for optimizing MSC therapy for PAD.

rather detrimental during reoxygenation. Coincidentally, apelin is capable of enhancing the protective autophagy in hypoxia, while suppressing the autophagic cell death in H/R. A combination of these properties appeared to be responsible for the ultimate protective effect of apelin against H/R injury.

Our data further depicted a possible role for the AMPK-mTOR-ULK1 signaling cascade in autophagy induction en route to the beneficial effects of apelin during hypoxia. The two protein complexes AMPK and mTORC1 are known to counter-regulate the autophagy inducing complex ULK1/2-Atg13-FIP200⁴²⁻⁴⁵. Under the low-energy conditions, AMPK positively regulates autophagy through inhibition of mTORC1. AMPK activation releases the inhibitory regulation of mTORC1 on the ULK1/2-Atg13-FIP200 complex, especially on ULK1/2 kinase activity⁴⁵. The AMPK/mTOR/ULK1 pathway represents an attractive target for therapeutic treatment of autophagy⁴⁶. In our hands, AMPK/mTOR/ULK1 pathway was up-regulated by apelin and may mediate protective autophagy under hypoxia *in vitro*. However, our *in vivo* data suggested that inhibition of AMPK/mTOR/ULK1 pathway using compound C failed to affect AD-MSCs survival as well as the combined therapeutic efficacy of AD-MSCs and apelin in experimental PAD. One plausible explanation may be that our *in vivo* experimental PAD model was more likely to be an ischemia/reperfusion process. After an initial short-period of ischemia, reperfusion process gradually took over (as evidenced by laser Doppler perfusion imaging for blood reperfusion). Thus the reperfusion process is deemed to be more critical than the initial short-period of ischemia in experimental PAD therapy.

Our study also demonstrated the Akt activation, Bcl2 activation to engage Beclin1 inhibition and suppressed autophagy en route to the beneficial action of apelin during reoxygenation, when AMPK is no longer active. Phosphorylation/activation of Akt kinase is known to regulate Bcl2, the Akt-Bcl2 pathway represents an important antiapoptotic signaling⁴⁷. Furthermore, Pattingre and colleagues reported that Bcl-2 antiapoptotic proteins inhibit Beclin 1-dependent autophagy, which is compatible with cell survival⁴⁸. Besides, Matsui and coworkers reported that suppressed autophagy via 3-MA or Beclin 1 knockout during reperfusion was accompanied by pronounced reduction in infarct size and apoptosis following simulated I/R⁴⁹. In our present work, apelin likely suppressed autophagic cell death through the Akt/Bcl2/Beclin1 pathway in H/R, thus promoting AD-MSCs survival under H/R injury. Our *in vivo* data also favored the notion that the Akt pathway seemed to be more important than AMPK pathway in apelin-improved functional survival and therapeutic efficacy of AD-MSCs. This may be attributed to our experimental PAD model as mentioned above. Taken together, the orchestration between AMPK and Akt signaling for autophagy seems to play a pivotal role in survival and function of AD-MSCs. These findings should help to shed some lights towards a better understanding of the protective role for apelin against I/R injury in ischemic hindlimbs.

Despite the clinical relevance of our findings, our study suffers from a number of limitations. For instance, although reporter gene imaging can be applied as a powerful tool for *in vivo* tracking of surviving stem cells, this technique is still limited within the laboratory⁵⁰. However, the translation of reporter gene imaging from bench to bedside is of great significance for the progress of stem cell therapy⁵⁰. Besides, the autophagy activity of engrafted AD-MSCs *in vivo* was not longitudinally evaluated for apparent technological reasons. *In vitro* H/R model may not fully mimic the ischemia/reperfusion microenvironment *in vivo*.

In summary, our work demonstrated a beneficial role of apelin in promoting the functional survival and therapeutic efficacy of AD-MSCs in stem cell based therapy for PAD. Apelin was shown to protect AD-MSCs against H/R injury, possibly via an AMPK-dependent induction of autophagy during hypoxia and an Akt-dependent suppression of autophagy during reoxygenation. This finding may warrant the consideration of a prospective clinical trial to evaluate the potential therapeutic impact of combined apelin-ADMSC treatment for patients with PAD to the conventional therapy.

Methods

Animals. Fluc⁺-eGFP⁺ double transgenic mice (Tg [Fluc-egfp]) were bred on a FVB/N background, which could constitutively express firefly luciferase (Fluc) and enhanced green fluorescence protein (eGFP) in all tissues and organs, and were used for AD-MSCs isolation^{4,51}. Syngeneic female FVB mice with the same genetic background as FVB mice (wide type, n = 360, 10-week-old, 20–25 g, SPF) were used for PAD model. This setting of cell recipients and cell donors should greatly minimize the immunogenicity raised by allogeneic MSCs⁵². All procedures were performed in accordance with the National Institutes of Health Guidelines on the Use of Laboratory Animal. Experimental protocols and animal care methods were approved by the Fourth Military Medical University Committee on Animal Care.

Isolation, Culture, and Identification of AD-MSCs^{Fluc+GFP+}. AD-MSCs^{Fluc+GFP+} were isolated from Fluc + -eGFP + double transgenic mice and expanded using our previously described procedure with minor modifications^{4,53}. Cultured AD-MSCs were identified for immunophenotype and multipotency using flow cytometry and chemical induction as we have previously described⁴.

Reporter gene imaging was performed to determine the stable expression of firefly luciferase (Fluc) in AD-MSCs. AD-MSCs of different quantities ranging from 1×10^5 to 10×10^5 were seeded into 96-well plates, suspended in 500 μ l phosphate-buffered saline (PBS), incubated with reporter probe D-luciferin (150 ng/ μ l, 88293, Invitrogen), and then imaged using a charge-coupled device (CCD) camera within Xenogen Kinetic *In vivo* Imaging System (IVIS, Caliper Life Sciences), with the following parameters: Binning: 4, F/Stop: 1, and Exposure time: 1 minute. Peak signal intensity was expressed in average radiance unit (photons/second/ cm^2 /steradian, $\text{P} \cdot \text{s}^{-1} \cdot \text{cm}^{-2} \cdot \text{sr}^{-1}$) from a fixed-area region of interest (ROI). LivingImage 4.2 software (Caliper, MA, USA) was used for imaging analysis.

H/R injury *in vitro*. Cultured AD-MSCs of third passage were stimulated with H/R injury as previously described⁵¹. Briefly, AD-MSCs were plated in 24-well plates (5×10^4 cells per well). Twenty-four hours later, AD-MSCs were administrated with PBS, cultured in Hanks buffer (GIBCO, 14025076). Then, different doses of apelin (ab141010, abcam, 10^{-10} , 10^{-8} , 10^{-6}) were added into respective wells for 6 hours. After that, AD-MSCs were incubated in an anoxic chamber (95% N₂/5% CO₂) (Thermo) at 37 °C for indicated period of time and subsequently moved or not moved (hypoxia only) into a normoxia incubator (95% air/5% CO₂) at 37 °C for indicated period of time, with refreshed cultured media. In the control group, AD-MSCs were maintained at normoxia (95% air, 5% CO₂) for equivalent periods.

Assessment of cell viability. Cell viability of cultured AD-MSCs were evaluated by both 3-(4,5-dimethylthiazol-2-yl)-2,5-diphenyltetrazolium bromide (MTT) assay and *in vitro* BLI. Briefly, cells were plated in 96-well plates at 1×10^4 /well. After hypoxia, H/R or normoxia treatment, cells from each group were harvested and incubated with 10 μ L MTT (KA1606, abnova, 5 g/L) for 4 h. After that, the incubation medium was removed and formazan crystals were dissolved in 150 μ L dimethyl sulphoxide (DMSO, BY12065, Sigma). The absorbance was determined at a wavelength of 490 nm.

For *in vitro* BLI, AD-MSCs were plated in 24-well plates (5×10^4 cells per well) for 24 h, followed by H/R or normoxia treatment, after that, firefly luciferase (Fluc) in AD-MSCs were detected by a charge-coupled device (CCD) camera within Xenogen Kinetic *In vivo* Imaging System (IVIS, Caliper Life Sciences) as described above.

PAD Model and Cell Delivery. FVB mice (n = 360) were randomized into nine groups (n = 40 each, matched for weight): (1) Sham group; (2) Sham + AD-MSCs group; (3) Sham + AD-MSCs + apelin group; (4) PAD + PBS group (PBS); (5) PAD + AD-MSCs group (AD-MSCs); (6) PAD + apelin group (apelin); (7) PAD + AD-MSCs + apelin group (AD-MSCs + apelin); (8) PAD + AD-MSCs + apelin + Compound C (AD-MSCs + apelin + Compound C); (9) PAD + AD-MSCs + apelin + LY294002 (AD-MSCs + apelin + LY294002). For the PAD model, unilateral hindlimb ischemia was induced by ligating and excising the left femoral artery with all superficial and deep branches for all groups except Sham. Surgical procedure for hindlimb ischemia is as previously described with minor modifications⁵. Sham-operated mice received incision without artery ligation or PBS treatment. Mice in the Sham + AD-MSCs, Sham + AD-MSCs + apelin, AD-MSCs, AD-MSCs + apelin, AD-MSCs + apelin + Compound C and AD-MSCs + apelin + LY294002 groups were subjected to AD-MSCs (1.0×10^7) delivery. Cells were suspended in 30 μ l PBS and cautiously injected into the left adductor muscle using a 29-gauge insulin syringe (324910, BD Biosciences). Sham + AD-MSCs + apelin, apelin, AD-MSCs + apelin, group animals were administered apelin-13 (1 mg/kg per day for consecutive 14 days from POD0, ab141010, abcam) via adductor injection, AD-MSCs + apelin + Compound C and AD-MSCs + apelin + LY294002 group animals were administered Compound C (50 nM/kg per day for consecutive 14 days from

POD0, 171260-10MG, EMD Millipore) or LY294002 (200 nM/kg per day for consecutive 14 days from POD0, 9901S, Cell Signaling Technology), respectively, via adductor injection, while PBS group animals received PBS only, without AD-MSCs.

***In vivo* BLI for AD-MSCs tracking.** *In vivo* BLI was performed to track the survival of engrafted AD-MSCs. Mice were anesthetized and intraperitoneally injected with 150 mg/kg D-luciferin(88293, Invitrogen). Using IVIS, images were acquired at 3-minute intervals until the peak signal was observed. Fixed-area region of interests(ROIs) were created over left hindlimbs, and photons emitted from the ROIs were quantified by $P\ s^{-1}cm^{-2}sr^{-1}$ using Living Image software (Caliper, MA, USA). Animals were longitudinally imaged at 0,1,3,5,7,10,14,21,28,35,42,49 days post operation.

***Ex vivo* Luciferase Assay.** Left adductor muscle tissues were removed from sacrificed mice on POD14, homogenized in PBS containing a protease inhibitor cocktail (B14001, Selleck), and lysed with $1 \times$ PLB (passive lysis buffer). After centrifugation at 15,000 rpm for 10 minutes at 4 °C, the supernatant was collected and then measured using the Luciferase Assay System for Luciferase activity.

Serial Laser Doppler Perfusion Imaging of Hindlimbs. Laser Doppler perfusion imaging (LDPI) was used to serially monitor the blood perfusion recovery of the ischemic hindlimbs. Briefly, mice were placed on a 37.4–38.0 °C heating pad to minimize temperature variation and then imaged using an analyzer (PeriScan-PIM3 Perimed AB, Sweden). The blood flux was quantified using perfusion ratio [PR, ratio of average LDPI index of ischemic to non-ischemic (contralateral, self-control) hindlimb] by LDPI win 3.1.3 (Perimed AB).

Blind scoring for murine ischemic damage and ambulatory impairment. Semiquantitative assessment of impaired use of murine ischemic limb was performed as previously described at different time points⁵⁴. Briefly, ischemic damage score were set as: 3 = dragging of foot, 2 = no dragging but no plantar flexion, 1 = plantar flexion, and 0 = flexing the toes to resist gentle traction on the tail. Ambulatory impairment score were set as: 0 = no difference from the right hindlimbs, 1 = mild discoloration, 2 = moderate discoloration, 3 = severe discoloration or subcutaneous tissue loss or necrosis, and 4 = any amputation. Amputation was defined as necrosis beyond the level of toes, including loss of ischemic lamb or loss of knees. All assessments were performed and averaged by 3 blinded and independent investigators.

Transmission electron microscopy. After indicated treatment, cultured AD-MSCs were collected and placed in a tube and centrifuged at 1,500 rpm for 10 min and the supernatant was carefully absorbed. The cells were then fixed with 3% glutaraldehyde(sc-358787, santacruz) and 1% osmium tetroxide (sc-206008, santacruz) for 24 h. Following rinsing with PBS for 30 min, the samples were dehydrated with ethanol and isopropanol, embedded in epoxy resin and prepared under a dissecting microscope. An ultrathin sectioning machine (Leica EM UC6, Leica Microsystems, Mannheim, Germany) was used to prepare the 1- μ m sections, then the samples were double stained with uranyl acetate and lead citrate. Ultrathin sections were observed using TEM (JEM-1200EX, JEOL Ltd., Tokyo, Japan). Images were captured and 10 randomly selected fields of vision from each group were used to quantify the area of the autophagosomes to the total cytoplasmic area.

Immunofluorescent staining. Immunofluorescence was performed to detect LC3 expression in AD-MSCs as well as AD-MSCs marker eGFP and angiogenesis marker CD31 in frozen sections of left adductor muscle. Briefly, frozen sections of left adductor muscle or cells were sequentially fixed within cold acetone for 10 min, washed three times with PBS containing 0.3% Triton X-100 and blocked with goat serum for 30 min at room temperature. Antibodies against LC3 (1:100; Cell Signaling Technology, #4108), GFP(1:2000, abcam, ab6556) and CD31(1:50; abcam, ab28364) was incubated overnight at 4 °C, followed by detection with corresponding fluorescent secondary anti-bodies (Santa Cruz Biotechnology, Santa Cruz, CA) for 1 h at 37 °C. Nuclei were counterstained with 49, 6-diamidino-2-phenylindole (DAPI, 4083S, Cell Signaling Technology). Slides were photographed by confocal microscope (FluoView-FV1000, Olympus, Japan). Image-Pro Plus 4.5 software (Media Cybernetics, Silver Spring, USA) were used to analyze fluorescence intensity.

Western blotting assay. After respective treatment, AD-MSCs were washed and scraped using lysis buffer[25 mM Tris-HCl (pH 7.4), 150 mM NaCl, 2 mM EDTA, 1% Triton-X-100, 1% sodium deoxycholate, 0.1% sodium dodecyl sulfate and protease inhibitor cocktail]. Samples consisting of 50 μ g total protein were loaded onto an SDS-PAGE gel(P0012AC, Beyotime) and transferred electrophoretically to nitrocellulose membranes (LC2000, invitrogen). After blocking with 5% bovine serum albumin in PBS, the membranes were incubated with the appropriate primary antibody against LC3 (#4108, Cell Signaling Technology,1:1000), p62 (ab56416, abcam,1:500), p AMPK α (ab13348, Anti-AMPK alpha 1 [phospho T183] + AMPK alpha 2 [phospho T172], abcam,1:1000), AMPK α (ab80089, abcam,1:1000), p-mTOR(#2971, Ser2448, Cell Signaling Technology, 1:2000), mTOR(#2972, Cell Signaling Technology, 1:2000), p-ULK1(#5869,Ser555, Cell Signaling Technology, 1:1000), ULK1(#8054,Cell Signaling Technology, 1:1000), p-Akt1(ab81283,Ser473,abcam,1:5000), Akt(ab32505, abcam,1:5000), Bcl-2(ab692, abcam,1:500), Beclin-1(ab16998, abcam,1:500) or ACTB (TA-09, Zhongshan Jinqiao Biotechnology Co.,1:2000) at 4 °C overnight. The next day, the blots were washed and incubated in the appropriate secondary antibodies(ab6721, ab6789, abcam) at room temperature for 1 h. Subsequent to being washed, the blots were developed and gray scale scanning (iBox Scientia 500/600, UVP, Upland, CA, USA) was performed. The expression levels of LC3, p62, Bcl-2 and Beclin-1 proteins were normalized to ACTB(β -actin). Quantitative analysis was performed using QuantiOne imaging software (Bio-Rad, USA) to assess the integrated optical density (IOD) of each band.

Statistical analysis. All analyses were performed with SPSS 20.0 software (SPSS Inc., Chicago, IL, USA). The measurement data are presented as mean \pm standard deviation (SD) and the multi-group comparisons were made with a one-way factor analysis of variance, followed by Dunnett's post hoc test. Data expressed as proportions were assessed with a Chi square test. Values of $P < 0.05$ were considered to indicate a statistically significant difference.

References

- Rooke, T. W. *et al.* 2011 ACCF/AHA focused update of the guideline for the management of patients with peripheral artery disease (updating the 2005 guideline): a report of the American College of Cardiology Foundation/American Heart Association Task Force on Practice Guidelines. *J Am Coll Cardiol(JACC)* **58**, 2020–2045 (2011).
- Lawall, H., Bramlage, P. & Amann, B. Stem cell and progenitor cell therapy in peripheral artery disease. *Thromb Haemost* **103**, 696–709 (2010).
- van der Bogt, K. E. *et al.* Molecular imaging of bone marrow mononuclear cell survival and homing in murine peripheral artery disease. *JACC: Cardiovasc Imag* **5**, 46–55 (2012).
- Fan, W. *et al.* Adipose stromal cell and sarpogrelate orchestrate the recovery of inflammation-induced angiogenesis in aged hindlimb ischemic mice. *Aging cell* **12**, 32–41 (2013).
- Pan, H., Cai, N., Li, M., Liu, G. H. & Izpisua Belmonte, J. C. Autophagic control of cell 'stemness'. *EMBO Mol Med* **5**, 327–331(2013).
- Guan, J.-L. *et al.* Autophagy in stem cells. *Autophagy* **9**, 830–849 (2013).
- Zhang, Q. *et al.* Autophagy activation: a novel mechanism of atorvastatin to protect mesenchymal stem cells from hypoxia and serum deprivation via AMP-activated protein kinase/mammalian target of rapamycin pathway. *Stem Cells Dev* **21**, 1321–1332 (2012).
- Shin, J. Y. *et al.* Mesenchymal stem cells enhance autophagy and increase β -amyloid clearance in Alzheimer disease models. *Autophagy* **10**, 32–44 (2014).
- Chen, J. *et al.* Melatonin attenuates inflammatory response-induced brain edema in early brain injury following a subarachnoid hemorrhage: a possible role for the regulation of pro-inflammatory cytokines. *J Pineal Res* **57**, 340–347 (2014).
- Haider, H. K. & Ashraf, M. Preconditioning and stem cell survival. *J Cardiovasc Transl* **3**, 89–102 (2010).
- Ravikumar, B. *et al.* Regulation of mammalian autophagy in physiology and pathophysiology. *Physiol Rev* **90**, 1383–1435 (2010).
- Marino, G. & Lopez-Otin, C. Autophagy: molecular mechanisms, physiological functions and relevance in human pathology. *CMLS-Cell Mol Life S* **61**, 1439–1454 (2004).
- Przyklenk, K., Dong, Y., Undyala, V. V. & Whittaker, P. Autophagy as a therapeutic target for ischaemia/reperfusion injury? Concepts, controversies, and challenges. *Cardiovasc Res* **94**, 197–205 (2012).
- Ma, S., Wang, Y., Chen, Y. & Cao, F. The role of the autophagy in myocardial ischemia/reperfusion injury. *BBA-Mol Basis Dis* **1852**, 271–276 (2015).
- Zhang, Q., Yao, F., Raizada, M. K., O'Rourke, S. T. & Sun, C. Apelin gene transfer into the rostral ventrolateral medulla induces chronic blood pressure elevation in normotensive rats. *Circ Res* **104**, 1421–1428 (2009).
- Japp, A. G. & Newby, D. E. The apelin-APJ system in heart failure: pathophysiologic relevance and therapeutic potential. *Biochem Pharmacol* **75**, 1882–1892 (2008).
- Lee, D. K. *et al.* Characterization of apelin, the ligand for the APJ receptor. *J Neurochem* **74**, 34–41 (2000).
- Kleinz, M. J. & Davenport, A. P. Emerging roles of apelin in biology and medicine. *Pharmacol Therapeut* **107**, 198–211 (2005).
- Simpkin, J. C. *et al.* Apelin-13 and apelin-36 exhibit direct cardioprotective activity against ischemiareperfusion injury. *Basic Res Cardiol* **102**, 518–528 (2007).
- Khaksari, M., Aboutaleb, N., Nasirinezhad, F., Vakili, A. & Madjd, Z. Apelin-13 protects the brain against ischemic reperfusion injury and cerebral edema in a transient model of focal cerebral ischemia. *J Mol neurosci* **48**, 201–208 (2012).
- Wang, W. *et al.* Loss of Apelin exacerbates myocardial infarction adverse remodeling and ischemia-reperfusion injury: therapeutic potential of synthetic Apelin analogues. *J Am Heart Assoc* **2**, e000249 (2013).
- Zeng, X., Yu, S. P., Taylor, T., Ogle, M. & Wei, L. Protective effect of apelin on cultured rat bone marrow mesenchymal stem cells against apoptosis. *Stem Cell Res* **8**, 357–367 (2012).
- Jiao, H., Zhang, Z., Ma, Q., Fu, W. & Liu, Z. Mechanism underlying the inhibitory effect of Apelin-13 on glucose deprivation-induced autophagy in rat cardiomyocytes. *Exp Ther Med* **5**, 797–802 (2013).
- Yang, L. *et al.* ERK1/2 mediates lung adenocarcinoma cell proliferation and autophagy induced by apelin-13. *Acta Bioch bioph Sin* **46**, 100–111 (2013).
- Vrtovec, B. *et al.* Comparison of transendocardial and intracoronary CD34+ cell transplantation in patients with nonischemic dilated cardiomyopathy. *Circulation* **128**, S42–S49 (2013).
- Silva, S. A. *et al.* Autologous bone-marrow mononuclear cell transplantation after acute myocardial infarction: comparison of two delivery techniques. *Cell Transplant* **18**, 343–352 (2009).
- Aranguren, X. L., Verfaillie, C. M. & Luttun, A. Emerging hurdles in stem cell therapy for peripheral vascular disease. *J Mol Med-JMM* **87**, 3–16 (2009).
- Robey, T. E., Saiget, M. K., Reinecke, H. & Murry, C. E. Systems approaches to preventing transplanted cell death in cardiac repair. *J Mol Cell Cardiol* **45**, 567–581 (2008).
- Zeng, X. J. *et al.* Apelin protects heart against ischemia/reperfusion injury in rat. *Peptides* **30**, 1144–1152 (2009).
- Tempel, D. *et al.* Apelin enhances cardiac neovascularization after myocardial infarction by recruiting aplnr + circulating cells. *Circ Res* **111**, 585–598 (2012).
- Lachmann, N. & Nikol, S. Therapeutic angiogenesis for peripheral artery disease: stem cell therapy. *Vasa* **36**, 241–251 (2007).
- Fan, W. *et al.* Adipose stromal cells amplify angiogenic signaling via the VEGF/mTOR/Akt pathway in a murine hindlimb ischemia model: a 3D multimodality imaging study. *PLoS one* **7**, e45621 (2012).
- Li, L., Li, L., Zhang, Z. & Jiang, Z. Hypoxia promotes bone marrow-derived mesenchymal stem cell proliferation through apelin/APJ/autophagy pathway. *Acta Bioch Bioph Sin* **47**, 362–367 (2015).
- Li, L. *et al.* Effects of apelin-13 on rat bone marrow-derived mesenchymal stem cell proliferation through the AKT/GSK3 β /cyclin D1 pathway. *Int J Pept Res Ther* **20**, 421–425 (2014).
- Zhang, J. *et al.* Apelin/APJ signaling promotes hypoxia-induced proliferation of endothelial progenitor cells via phosphoinositide-3 kinase/Akt signaling. *Mol Med Rep* **12**, 3829–3834, (2015).
- Li, L., Zeng, H. & Chen, J. X. Apelin-13 increases myocardial progenitor cells and improves repair postmyocardial infarction. *Am J Physiol Heart Circ Physiol* **303**, H605–618 (2012).
- Masri, B., Morin, N., Cornu, M., Knibiehler, B. & Audigier, Y. Apelin (65–77) activates p70 S6 kinase and is mitogenic for umbilical endothelial cells. *Faseb J* **18**, 1909–1911 (2004).
- Cui, R.-R. *et al.* Apelin suppresses apoptosis of human vascular smooth muscle cells via APJ/PI3-K/Akt signaling pathways. *Amino acids* **39**, 1193–1200 (2010).
- Codogno, P. & Meijer, A. J. Autophagy and signaling: their role in cell survival and cell death. *Cell Death Differ* **12**, 1509–1518 (2005).

40. Sekiguchi, A., Kanno, H., Ozawa, H., Yamaya, S. & Itoi, E. Rapamycin promotes autophagy and reduces neural tissue damage and locomotor impairment after spinal cord injury in mice. *J Neurotraum* **29**, 946–956 (2012).
41. Noh, H. S. *et al.* Propofol protects the autophagic cell death induced by the ischemia/reperfusion injury in rats. *Mol Cells* **30**, 455–460 (2010).
42. Meley, D. *et al.* AMP-activated protein kinase and the regulation of autophagic proteolysis. *J Biol Chem* **281**, 34870–34879 (2006).
43. Sengupta, S., Peterson, T. R. & Sabatini, D. M. Regulation of the mTOR complex 1 pathway by nutrients, growth factors, and stress. *Mol Cell* **40**, 310–322 (2010).
44. Wullschleger, S., Loewith, R. & Hall, M. N. TOR signaling in growth and metabolism. *Cell* **124**, 471–484 (2006).
45. Alers, S., Löffler, A. S., Wesselborg, S. & Stork, B. Role of AMPK-mTOR-Ulk1/2 in the regulation of autophagy: cross talk, shortcuts, and feedbacks. *Mol Cell Biol* **32**, 2–11 (2012).
46. Meric-Bernstam, F. & Gonzalez-Angulo, A. M. Targeting the mTOR signaling network for cancer therapy. *J Clin Oncol* **27**, 2278–2287 (2009).
47. Asnaghi, L. *et al.* Bcl-2 phosphorylation and apoptosis activated by damaged microtubules require mTOR and are regulated by Akt. *Oncogene* **23**, 5781–5791 (2004).
48. Pattingre, S. *et al.* Bcl-2 antiapoptotic proteins inhibit Beclin 1-dependent autophagy. *Cell* **122**, 927–939 (2005).
49. Matsui, Y. *et al.* Distinct roles of autophagy in the heart during ischemia and reperfusion: roles of AMP-activated protein kinase and Beclin 1 in mediating autophagy. *Circ Res* **100**, 914–922 (2007).
50. Nguyen, P. K., Riegler, J. & Wu, J. C. Stem cell imaging: from bench to bedside. *Cell stem cell* **14**, 431–444 (2014).
51. Fan, W. *et al.* mTORC1 and mTORC2 play different roles in the functional survival of transplanted adipose-derived stromal cells in hind limb ischemic mice via regulating inflammation *in vivo*. *Stem cells* **31**, 203–214 (2013).
52. Huang, X. P. *et al.* Differentiation of allogeneic mesenchymal stem cells induces immunogenicity and limits their long-term benefits for myocardial repair. *Circulation* **122**, 2419–2429 (2010).
53. Han, D. *et al.* Ghrelin Improves Functional Survival of Engrafted Adipose-Derived Mesenchymal Stem Cells in Ischemic Heart through PI3K/Akt Signaling Pathway. *Biomed Res Int* **2015**, e858349 (2015).
54. Stabile, E. *et al.* Impaired arteriogenic response to acute hindlimb ischemia in CD4-knockout mice. *Circulation* **108**, 205–210 (2003).

Acknowledgements

This work was supported by Beijing Nature Science Foundation (No. 7152131), the National Funds for Distinguished Young Scientists of China (No. 81325009), National Nature Science Foundation of China (No. 81270168, 81530058, 81227901), (FCao BWS12J037) and Innovation Team Grant of Shanxi Province (No. 2014KCT-20).

Author Contributions

F.C., J.R., D.L. and D.H. designed the research study; D.L., D.H., W.F., R.Z., H.Y.Q. and S.M. performed the experiments; X.L., W.F. and R.Z. analyzed the data; J.R., D.H. and D.L. wrote the paper; J.C. and Y.W. participated in the conception of the study and revision of the manuscript. All authors approve of the final version to be published.

Additional Information

Supplementary information accompanies this paper at <http://www.nature.com/srep>

Competing financial interests: The authors declare no competing financial interests.

How to cite this article: Liang, D. *et al.* Therapeutic efficacy of apelin on transplanted mesenchymal stem cells in hindlimb ischemic mice *via* regulation of autophagy. *Sci. Rep.* **6**, 21914; doi: 10.1038/srep21914 (2016).



This work is licensed under a Creative Commons Attribution 4.0 International License. The images or other third party material in this article are included in the article's Creative Commons license, unless indicated otherwise in the credit line; if the material is not included under the Creative Commons license, users will need to obtain permission from the license holder to reproduce the material. To view a copy of this license, visit <http://creativecommons.org/licenses/by/4.0/>